AD-A187 001 GEOMETRIC STRUCTURE PSEUDOBAND GAPS AND SURFACE VIBRATIONAL RESONANCES ON (U) CORNELL UNIV ITHACA NY LAB OF ATOMIC AND SOLID STATE PHYSICS

UNCLASSIFIED M PERSSON ET AL AUG 87 TR-40 F/G 7/4 NL

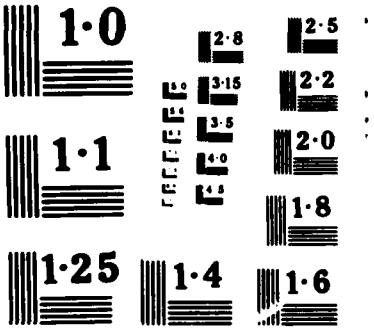
1·0
1·1
1·25
1·4
2·8
3·15
3·5
2·5
2·2
2·0
1·8
1·6

OFFICE OF NAVAL RESEARCH

Contract N00014-82-K-0576

Technical Report No. 40

Geometric Structure, Pseudoband Gaps, and Surface Vibrational Resonances on Metal Surfaces

by

M. Persson, J. A. Stroscio and W. Ho

LASSP
Cornell University
Ithaca, NY

August 1987

A187 001

SECURITY CLASSIFICATION OF THIS PAGE (When Data Entered)

REPORT DOCUMENTATION PAGE

READ INSTRUCTIONS BEFORE COMPLETING FORM

1. REPORT NUMBER	2. GOVT ACCESSION NO.	3. RECIPIENT'S CATALOG NUMBER
40		

4. TITLE (and Subtitle)	5. TYPE OF REPORT & PERIOD COVERED
Geometric Structure, Pseudoband Gaps, and Surface Vibrational Resonances on Metal Surfaces	Technical Report
	6. PERFORMING ORG. REPORT NUMBER

7. AUTHOR(s)	8. CONTRACT OR GRANT NUMBER(s)
M. Persson, J. A. Stroscio, W. Ho	N00014-82-K-0576

9. PERFORMING ORGANIZATION NAME AND ADDRESS	10. PROGRAM ELEMENT, PROJECT, TASK AREA & WORK UNIT NUMBERS
Laboratory of Atomic and Solid State Physics Cornell University Ithaca, NY 14853-2501	

11. CONTROLLING OFFICE NAME AND ADDRESS	12. REPORT DATE
Office of Naval Research 800 Quincy St., Arlington VA	August 1987
	13. NUMBER OF PAGES 11

14. MONITORING AGENCY NAME & ADDRESS(if different from Controlling Office)	15. SECURITY CLASS. (of this report)
	15a. DECLASSIFICATION/DOWNGRADING SCHEDULE

16. DISTRIBUTION STATEMENT (of this Report)

This document has been approved for public release and sale; its distribution is unlimited.

17. DISTRIBUTION STATEMENT (of the abstract entered in Block 20, if different from Report)

18. SUPPLEMENTARY NOTES

19. KEY WORDS (Continue on reverse side if necessary and identify by block number)

20. ABSTRACT (Continue on reverse side if necessary and identify by block number)

It is shown by surface lattice dynamics that a new type of surface vibrational resonance arises in those frequency regions where there is a strong depletion in the bulk phonon density of states. The presence of these pseudoband gaps is due to higher Fourier components in the phonon dispersion relations introduced by the particular coordination of atoms in layers parallel to the surface. A quantitative analysis based on surface lattice dynamics of the recorded electron energy loss spectra of Cu and Ni suggests that the outermost surface interlayer force constant is rather close to the bulk value. This resonance is found to exist throughout the X direction

DD FORM 1473 EDITION OF 1 NOV 65 IS OBSOLETE
S/N 0102-014-6601

(SEE BACK)

SECURITY CLASSIFICATION OF THIS PAGE (When Data Entered)

and makes an avoided crossing with a resonance derived from a band gap at the X point. An explanation is given for the disappearance of the divergent van Hove singularities in theprojected bulk density of states upon projection on a surface layer.

Geometric Structure, Pseudoband Gaps, and Surface Vibrational Resonances on Metal Surfaces

M. Persson,* Joseph A. Stroscio† and W. Ho

Laboratory of Atomic and Solid State Physics and Materials Science Center, Cornell University, Ithaca, New York 14853-2501, U.S.A.

Received January 22, 1987; accepted January 30, 1987

Abstract

It is shown by surface lattice dynamics that a new type of surface vibrational resonance arises in those frequency regions where there is a strong depletion in the bulk phonon density of states. The presence of these pseudoband gaps is due to the higher Fourier components in the phonon dispersion relations introduced by the particular coordination of atoms in layers parallel to the surface. A quantitative analysis based on surface lattice dynamics of the recorded electron energy loss spectra of Cu and Ni suggests that the outermost surface interlayer force constant is rather close to the bulk value. This resonance is found to exist throughout the $\bar{\Gamma}\bar{X}$ direction and makes an avoided crossing with a resonance derived from a band gap at the $\bar{X}$-point. An explanation is given for the disappearance of the divergent van Hove singularities in the projected bulk density of states upon projection on a surface layer.

1. Introduction

The vibrational properties of clean metal surfaces have recently attracted a lot of attention both from an experimental and theoretical point of view. These studies have been made possible by new surface sensitive vibrational spectroscopies such as inelastic He scattering and electron energy loss spectroscopy (EELS). These techniques probe vibrations with such high frequencies that the surface lattice dynamics cannot be described fully within the continuum elasticity theory. In this frequency regime the atoms vibrate with large relative displacements such that the surface geometric structure and the surface interatomic forces are expected to play a decisive role. Recent measurements on Ni(100) by EELS [1, 2] and Ag(111) by inelastic He scattering [3, 4] demonstrated that such information can be extracted from surface vibrational spectra.

The possibility to observe dipole active surface vibrational modes on clean metal surfaces was recently demonstrated for the (100) surfaces of Cu and Ni by EELS [5]. In a recent letter we reported the observation of dipole active resonance modes on the (110) surfaces of Cu and Ni [6]. These modes were shown from surface lattice dynamics calculations to be a new kind of resonance arising from a pseudoband gap in the density of states for longitudinal phonons propagating normal to the surface. This gap defines a region where the bulk phonon density of states is significantly depleted and has a simple structural explanation in terms of the coordination of the atoms in the layers normal to the (110) direction of fcc crystals. A recent analysis of the bcc(111) surface has shown that this type of surface resonance is a general effect which results from higher harmonic terms in the bulk phonon dispersion relations introduced by the particular coordination of atoms in the layers parallel to the surface [7].

In this paper we show in detail how a surface vibrational resonance arises in situations with pseudoband gaps in the bulk phonon density of states. The surface is observed to split off a mode from the region of high density of bulk phonon states into the pseudoband gap region where the strong depletion of the density of states causes the mode to become a resonance. An argument is also given for explaining why the divergent van Hove singularities which are present in the projected bulk density of states disappear for a projection on the surface layers. These divergences disappear because an incident phonon at those frequencies interfere destructively with the phonons scattered from the surface. On the [110] surfaces of fcc Ni and Cu crystals the pseudoband gap is shown to exist along the $\bar{\Gamma}\bar{X}$ direction in the surface Brillouin zone (SBZ). The corresponding surface vibrational resonance makes an avoided crossing with a resonance derived from a gap mode at the $\bar{X}$-point in the SBZ.

A detailed quantitative comparison of the measured spectra with the calculated EEL spectra show that the loss peak derived from the resonance is reproduced with a value for the outermost surface interlayer force constant within $\pm 15\%$ from its bulk value. In contrast, large oscillatory relaxations of the surface layers were observed by low energy electron diffraction (LEED) for these surfaces [8]. The EEL spectra also give information about the dipole activity of the surface layers. The shape of the loss spectrum is well reproduced by only the two outermost surface layers giving the dominant contribution to the dipole activity. The dipole strength is found to be of the same order of magnitude as measured for the (100) surfaces [5].

The vibrational structures of the surface appear in the measured spectra through a specific projection of the surface vibrational density of states. While the relevant projection probed in inelastic He scattering is essentially given by the displacements of the outermost surface atoms normal to the surface [9], the relative rigid displacements of the surface layers is the relevant projection in inelastic dipole scattering [5]. Such vibrational density of states have been evaluated here from surface lattice dynamics for a semi-infinite substrate using simple force constant models.

The force constant models have been extracted from Born von Karman analysis of inelastic neutron scattering data with particular emphasis on the high frequency vibrations. The bulk phonon dispersions of Cu and Ni are well described by a single nearest neighbouring force constant [10, 11]. The surface force constants have been chosen to have the same values as the bulk layers. This choioce should be viewed as

* Permanent address: Institute of Theoretical Physics, Chalmers University of Technology, S-412 96 Göteborg, Sweden.

† Present address: IBM, T J. Watson Research Center, Yorktown Heights, NY 10598, U.S.A.

a reference model with no more justification than that it describes the large effect of the loss of coordination of atoms at the surface.

The surface vibrational density of states has been calculated using a Green's function technique proposed by Lee and Joannopoulos [12]. This technique is based on the transfer matrix and its application to surface lattice dynamics is described in the Appendix.

2. Experimental procedures

The experiments were performed in a multitechnique ultrahigh vacuum system which is evacuated by turbomolecular, ion, and titanium sublimation pumps with a base pressure of 4×10^{-11} Torr [13]. The electron spectrometer is based on a double pass 127° cylindrical electrostatic deflector for the monochromator and analyzer. The scattering geometry is fixed with a total scattering angle of 120°. The angular acceptance of the analyzer is 1.8° at full-width-half-maximum (FWHM). The scattering plane containing the incident and scattered electrons is defined by the surface normal and the [1$\bar{1}$0] crystallographic direction for the Cu(110) and Ni(110) surfaces. The spectra were recorded in the specular direction at a temperature of 300 K. Impact energies of 3.2 and 4.3 eV were used for Cu and Ni respectively.

The samples, which were approximately 1 cm diam and 1 mm thick disks, were cleaned by neon ion bombardment (500 eV) and annealing to 750 and 1050 K for Cu and Ni, respectively. The samples were spotwelded to a manipulator with a pair of 0.5 mm Ta wires for the Ni samples and with 0.5 mm Pt wires for the Cu sample. The clean surfaces displayed sharp 1 × 1 LEED patterns without any sign of typical impurity vibrations, such as O, C, or S, in the electron energy loss spectra.

The vibrational spectra of the clean Cu and Ni(110) surfaces are shown in Fig. 1. A single sharp vibrational loss peak is observed at 20 and 24 meV on the Cu(110) and Ni(110) surfaces, respectively. Off-specular measurements show these losses to be excited by the dipole scattering mechanism [14]. Energy gain peaks are also observed with an intensity ratio to the energy loss peaks determined by the Bose–Einstein distribution factor at 300 K. An important feature of these losses is that the ratio of their energies scales as the ratio of the maximum bulk phonon frequency which is 29.7 and 36.7 meV for Cu [10] and Ni [11], respectively. This fact suggests that these losses are derived from longitudinal phonons propagating normal to the surface.

3. Pseudoband gaps and surface resonances

The notion of a pseudoband gap is illustrated by the dispersion of longitudinal bulk phonons in the [110] direction. A detailed analysis of the displacement fields for phonons scattered from the surface shows how a surface vibrational resonance can develop in this situation and why the divergent van Hove singularities present in the projected bulk phonon density of states disappear on the surface projection. The development of a resonance on the (110) surface is contrasted with the (100) and (111) surfaces where no such resonances appear within the nearest neighbor central force constant model.

For the (110) surface of fcc metals only rigid motions of

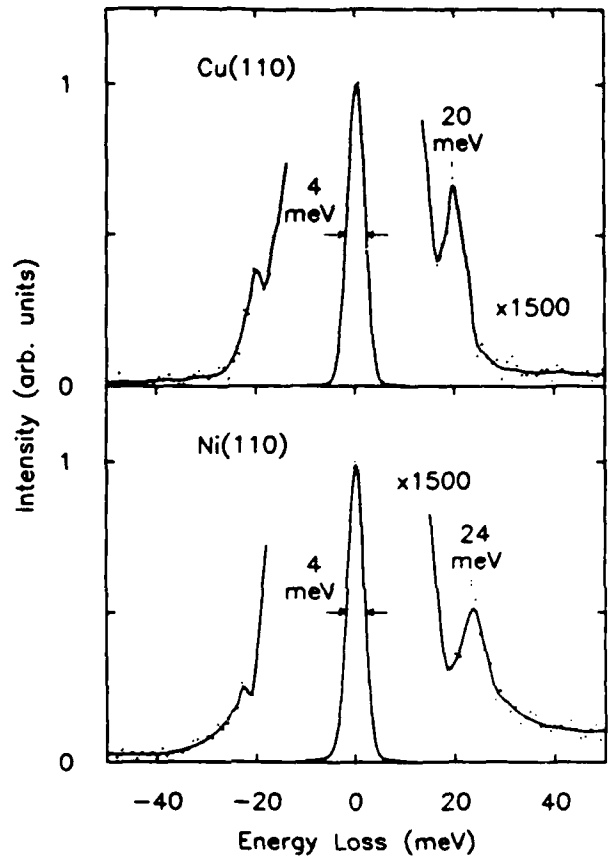

Fig. 1. Electron energy loss spectra of the clean (110) surfaces of Cu and Ni. The specra were recorded in the specular direction at 300 K. The sharp peaks observed at 20 and 24 meV, for Cu and Ni respectively, correspond to surface vibrational resonances.

the layers of atoms normal to the surface can be dipole active. Such a motion of the bulk layers corresponds to longitudinal bulk phonons propagating in the [110] direction. It is known since the early studies by inelastic neutron scattering that the full bulk phonon dispersions for Cu and Ni can be well described by a Born–von Karman model of lattice dynamics based on central nearest neighboring force constants [10, 11]. In this model the eigenvalue problem for the longitudinal bulk phonons propagating in the [110] direction is given by

$$\omega^2 w_L = \frac{\alpha}{M}(4w_L - w_{L+1} - w_{L-1} - w_{L+2} - w_{L-2}), \quad (1)$$

and is in the [100] and [111] directions given by

$$\omega^2 w_L = \frac{2\alpha}{M}(2w_L - w_{L+1} - w_{L-1}), \quad (2)$$

where w_L is the displacement of an atom in the Lth layer in a direction normal to the layer, ω the frequency, α the central nearest neighboring force constant, and M the mass of an atom.

From the translational symmetry of the bulk layers the solutions to eqs. (1) and (2) are simple plane waves $w_l = e^{i\zeta L}$ with energies $\omega(\zeta)$ satisfying the dispersion relation for the [110] direction,

$$\omega^2(\zeta) = \frac{\omega_0^2}{2}\left[\sin^2\left(\frac{\pi\zeta}{2}\right) + \sin^2(\pi\zeta)\right], \quad (3)$$

and for the [100] and [111] directions,

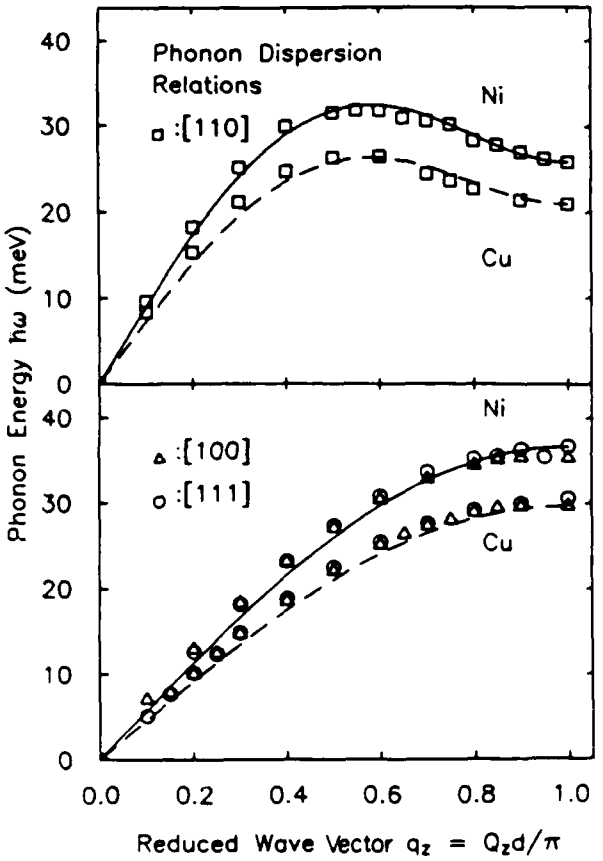

Fig. 2 Longitudinal bulk phonon dispersion relations in the [110], [111] and [100] directions of Cu and Ni. The data from inelastic neutron scattering are compared with results from a nearest neighbor central force constant model. The interlayer distance is d.

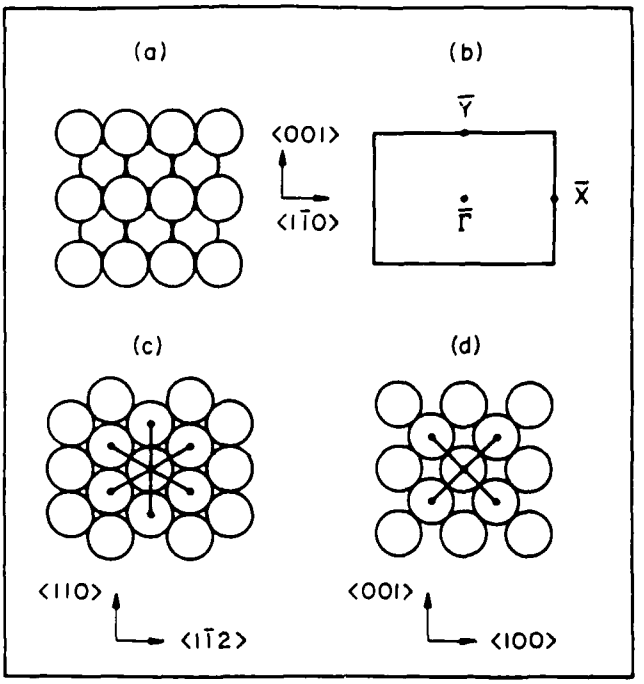

Fig. 3 Structure of fcc crystals in the [110] and [100] directions. (a) Top view of atoms of the (110) surface together with the crystallographic directions. The (110) surface Brillouin zone is depicted in (b). The coordination of atoms in the bulk layers normal to the surface are shown for (c) the [110] and (d) the [100] directions.

$$\omega^2(\zeta) = \omega_0^2 \sin^2\left(\frac{\pi\zeta}{2}\right), \tag{4}$$

where $\omega_0^2 = 8\alpha/M$. The resulting phonon dispersion from this simple force constant model for the lattice dynamics agrees fairly well with data from inelastic neutron scattering for all the major crystallographic directions as shown in Fig. 2 when ω_0 is adjusted so that $\omega(\zeta = 1)$ is equal to the measured value in the [110] direction, i.e., $\omega(\zeta = 1) = \omega_0/\sqrt{2}$, $\omega_0 = 29.7$ and 36.7 meV for Cu and Ni, respectively. The fit is particularly good in the high energy region and the largest discrepancies are typically found in, for this analysis, the less interesting low energy region.

A characteristic feature of the dispersion in the [110] direction is its non-monotonic behavior with a maximum at $\zeta = \zeta_m$, well within the Brillouin zone. This behavior can be understood simply from the coordination of atoms in this direction shown in Fig. 3. In this case an atom has nearest neighbors not only in the nearest layer but also in the next nearest layer. The next nearest neighboring atom lies in the [110] direction and causes the next nearest interlayer force constant to be as strong as the nearest interlayer force constant in eq. (1). This causes for instance the restoring force for the displacement fields at $\zeta = 0.5$ to be stronger than at $\zeta = 1.0$. In the other two crystallographic directions an atom has only nearest neighboring atoms in the nearest neighboring layer and this causes the dispersion to be monotonic with ζ as evidenced by eqs. (2) and (4).

In surface vibrational spectroscopy one probes the vibrational density of states in the surface region. Before presenting results for the surface density of states we will consider first the density of states for a bulk layer. The phonon density of state $g(\omega)$ for a bulk layer is simply determined by

$$g(\omega) = \sum_i \left|\frac{d\omega}{d\zeta}\right|^{-1}_{\zeta=\zeta_i}, \tag{5}$$

where the sum is over all positive ζ_i satisfying $\omega = \omega(\zeta_i)$. From the phonon dispersion relations given by eqs. (3) and (4) $g(\omega)$ can be evaluated straightforwardly and is presented for Ni in Fig. 4 (upper panel). In the low energy limit $\omega = c_L\zeta\pi/d$ and $g(\omega)$ goes to a constant, $g(\omega) \approx d/c_L\pi$, where c_L is the longitudinal sound velocity and d the interlayer spacing. In one-dimensional problems, as in the case considered here, the stationary points in the dispersion relation defined by $d\omega/d\zeta = 0$ give rise to divergent van Hove singularities in $g(\omega)$ [15]. The divergences are in most cases power singularities with an exponent $-1/2$. This kind of singular behavior is readily shown from the fact that it is possible to make a Taylor expansion $\omega(\zeta) \simeq \omega_s + \gamma(\zeta - \zeta_s)^2/2$ around an isolated stationary point $\zeta = \zeta_s$ and eq. (5) gives directly that

$$g(\omega) \simeq \frac{1}{\sqrt{2|\gamma|}}\,|\omega - \omega_s|^{-1/2}, \quad \zeta \to \zeta_s. \tag{6}$$

However, in some exceptional cases, which are not encountered here, $\gamma = 0$ and the next leading term in the Taylor expansion gives rise to another value for the exponent. For metals it is also possible to have non-analytical behavior, Kohn anomalies, from the long-range interactions introduced by the sharp Fermi surface. These singularities are not discernible for Cu and Ni. The most important point to be made here about $g(\omega)$ is the fact that the [110] dispersion relation has a relatively large density of states in a rather narrow region in ω, $22 \lesssim \hbar \lesssim 33$ meV, compared to the low

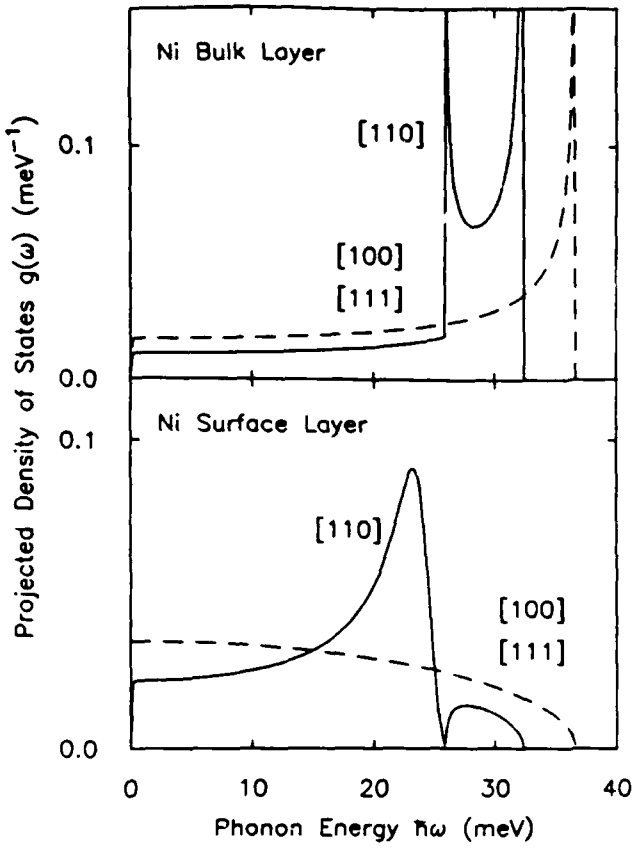

Fig. 4. The density of states $g(\omega)$ for longitudinal phonons projected on bulk and surface layers for Ni. The results for $g(\omega)$ in the [110], [111] and [100] crystal directions have been calculated using the same force constant model as in Fig. 1.

energy region $0 \leqslant \hbar \lesssim 22\,\text{meV}$. This latter region will for that reason be called a psuedoband gap. No such region can be defined for the other two directions [110] and [111].

In order to evaluate $g(\omega)$ for a surface layer one needs a model for the effects of the surface on the force constants. An obvious effect of forming a surface is the corresponding loss of coordination of the surface atoms. Here we will only account for that effect on the interlayer force constant. The resulting equations describing the surface layers in the [110] direction are given by,

$$\begin{aligned} \omega^2 w_1 &= \frac{\alpha}{M}(2w_1 - w_2 - w_3) \\ \omega^2 w_2 &= \frac{\alpha}{M}(3w_2 - w_1 - w_3 - w_4), \end{aligned} \tag{7}$$

and for the outermost surface layers in the [100], [111] direction

$$\omega^2 w_1 = \frac{2\alpha}{M}(w_1 - w_2). \tag{8}$$

Note that within this formalism the relaxation of the surface layers is taken into effect only through modifications of the surface interlayer force constants.

The presence of the surface breaks the translational symmetry and the solutions to eqs. (1) and (7) can no longer be written as a single plane wave. Rather a wave $e^{-i\pi\zeta L}$ incident on the surface will be reflected and can couple to another wave $e^{+i\pi\tilde{\zeta}L}$ with the same energy $\omega(\tilde{\zeta}) = \omega(\zeta)$. This kind of argument suggests the following ansatz for the scattered wave in the [110] direction,

$$w_L = e^{-i\pi\zeta L} + R(\zeta)\, e^{i\pi\zeta L} + \tilde{R}(\zeta)\, e^{+i\pi\tilde{\zeta}L}. \tag{9}$$

This form for the ansatz is justified in the Appendix. Due to the non-monotonic behavior of the dispersion some care is needed to get the right boundary conditions. The reduced wavevector ζ has to be chosen from the ranges $-1 \leqslant \zeta < -\zeta_m$ and $0 \leqslant \zeta < \zeta_m$ where the maximum in the phonon dispersion occurs at $\pm\zeta_m$. In these ranges the group velocity is positive, $d\omega/d\zeta > 0$, so that $e^{-i\pi\zeta L}$ and $e^{i\pi\zeta L}$ are incoming and outgoing waves, respectively. The other reflected wave $e^{+i\pi\tilde{\zeta}L}$ is propagating for $\omega/\omega_0 \geqslant 1/\sqrt{2}$ and similarly has to be chosen from the ranges where the group velocity is positive, $d\omega/d\tilde{\zeta} > 0$. For smaller energies $\omega/\omega_0 < 1/\sqrt{2}$, $\tilde{\zeta}$ is complex and $e^{i\pi\tilde{\zeta}L}$ is an evanscent wave and the sign of $\text{Im}\,\tilde{\zeta}$ has to be chosen so that it is a decaying wave.

The two reflection coefficients $R(\zeta)$ and $\tilde{R}(\zeta)$ are now determined from the two equations of motion for the surface layers, eq. (7). The two equations for $R(\zeta)$ and $\tilde{R}(\zeta)$ are given by,

$$d_i(\zeta)R(\zeta) + d_i(\tilde{\zeta})\tilde{R}(\zeta) = -d_i(-\zeta), \quad i = 1, 2 \tag{10}$$

where

$$d_1(\zeta) = (\nu^2(\zeta) - 1/4) + \tfrac{1}{8}(e^{i\pi\zeta} + e^{i2\pi\zeta})$$

and

$$d_2(\zeta) = (\nu^2(\zeta) - 3/8) + \tfrac{1}{8}(e^{-i\pi\zeta} + e^{i\pi\zeta} + e^{i2\pi\zeta}).$$

Here ν is the reduced energy $\nu = \omega/\omega_0$. The surface vibrational density of states defined as,

$$g(\omega) = \int_0^1 d\zeta\, |w_1|^2 \delta[\omega - \omega(\zeta)] \tag{11}$$

can now be evaluated from eq. (9). It turns out, however, that it is more elegant and practical to evaluate $g(\omega)$ by the transfer matrix method described in detail in the Appendix. The resulting $g(\omega)$ calculated by the transfer matrix method for the [110] direction is depicted in Fig. 4 (lower panel).

A noteworthy feature of $g(\omega)$ is that the divergent van Hove singularities have disappeared in the projection on the outermost surface layer. This can be shown rather easily from eqs. (9) and (10) to be due to the fact that one gets destructive interference between incident and reflected waves resulting in $w_L \equiv 0$ at the stationary points. For instance at $\zeta = \zeta_m$ the ansatz degenerates to

$$w_L = [1 + \tilde{R}(\zeta_m)]\, e^{-i\pi\zeta_m L} + R(\zeta_m)\, e^{+i\pi\zeta_m L}. \tag{12}$$

Instead of having two inhomogeneous equations for $\tilde{R}(\zeta)$ and $R(\zeta)$ from eq. (10) we have now two homogeneous equations for $1 + \tilde{R}(\zeta_m)$ and $R(\zeta_m)$. These two equations will in general have a trivial solution except in those accidental cases where the determinant is identically zero. Thus the contribution of $g(\omega)$ from $\zeta = \zeta_m$ is $g(\omega) = |w_1(\zeta)|^2/|d\omega/d\zeta|$. From eq. (10) it is evident that $w_1(\zeta)$ is analytic around $\zeta = \zeta_m$, and $w_1(\zeta) \simeq \lambda(\zeta - \zeta_m)$ since $w_1(\zeta_m) = 0$. Similarly for $\omega(\zeta)$, $\omega(\zeta) \simeq \omega_m + \gamma(\zeta - \zeta_m)^2/2$, and

$$g(\omega) \simeq \frac{\sqrt{2}|\lambda|^2}{|\gamma|^{1/2}}(\omega_m - \omega)^{1/2}, \quad \zeta \to \zeta_m. \tag{13}$$

Thus the divergent van Hove singularity $\sim(\omega - \omega_m)^{-1/2}$ at a bulk layer for the one-dimensional model turns into a bounded van Hove singularity $\sim(\omega - \omega_m)^{1/2}$ on a surface

layer. This argument indicates also that the divergent van Hove singularity should not exist in $g(\omega)$ for a projection on any layer for the semi-infinite substrate. A closer analysis reveals, however, that the bulk density of states are recovered in the limit $L \to \infty$. For instance, for a layer far inside, $L \gg 1$, $|w_L|^2 \simeq 4 \sin^2[\pi(\zeta - \zeta_m)L]$ when $\zeta \to \zeta_m$. Thus $g(\omega)$ will rise rapidly when going away from ω_m and have a large maximum $8L/|\gamma|$ at $\zeta - \zeta_m = 1/2L$, arbitrarily close to ω_m. This argument for the disappearance of the divergent van Hove singularities in a projection of $g(\omega)$ on a surface layer can be shown to apply to more general situations. For instance, it is not necessary that surface force constants are the same as in the bulk region.

Most importantly, $g(\omega)$ shows a sharp narrow feature around 23 mV as seen in Fig. 4 (lower panel). This feature is now shown to be a surface vibrational resonance. In a situation where there is an absolute band gap it is well known that the surface can introduce a localized state split off from the band. In the present case there is no absolute band gap rather a pseudoband gap. The surface can possibly split off a state from the band which turns into a resonance by overlapping with the low density of bulk states in the pseudoband gap. This expectation is confirmed from an analysis of the reflection coefficient for $\omega/\omega_0 < 1/\sqrt{2}$, $\zeta = 1 + i\kappa$ where $\cosh \pi\kappa = \frac{1}{4}[1 + \sqrt{25 - 32(\omega/\omega_0)^2}]$ and the complex part gives rise to an evanescent wave $(-1)^L e^{-\kappa L}$. The corresponding reflection coefficient $\tilde{R}(\zeta)$ is found to have a simple pole for complex ν at $\nu_{pole} = 0.663 + i0.047$ (for Ni, $\hbar\omega_{pole} = (24.3 + i1.73)$ meV). The existence of such a pole with an imaginary part ω_i relatively close to the real axis justifies calling this rather sharp peak a surface vibrational resonance. Note that the peak is quite asymmetrical due to interference with bulk states in the depicted projection, a feature which is typical for Fano-resonances [16].

For the [100] and [111] directions the ansatz for the solution to eqs. (2) and (8) has a more simple form

$$w_L = e^{i\pi\zeta L} + R(\zeta)\, e^{-i\pi\zeta L} \tag{14}$$

for $0 \leqslant \zeta \leqslant 1$. This ansatz inserted into eq. (8) for the surface layer gives a simple form for the reflection coefficient $R(\zeta) = e^{i\pi\zeta}$. As a function of ν this reflection coefficient, $R(\zeta) = 1 - 2\nu^2 + 2i\sqrt{\nu^2 - \nu^4}$ (when $0 < \zeta < 1$), has no poles associated with any resonances. The phonon density of states $g(\omega)$ projected on a surface layer can now be evaluated directly from eq. (11) and is given by

$$g(\omega) = \frac{4}{\pi}\sqrt{1 - (\omega/\omega_0)^2}. \tag{15}$$

This density of states shows accordingly no surface vibrational resonances as depicted in the lower panel of Fig. 4.

4. Comparison with experiment

An attractive feature of EELS is the possibility to analyze quantitatively the measured dipole active losses [17]. The dipole loss function for longitudinal bulk phonons is calculated for Ni and compared with the measured spectrum. The sensitivity of the calculated spectra to changes in the surface force constant and the distribution of the dipole activity among the surface layers are also investigated.

In a recent letter it was shown both experimentally and theoretically that the displacements of the outer layers of metal atoms can give rise to a long range dipole field due to incomplete screening by the conduction electrons of the electric field from the displaced ion cores [5]. The strength of the dipole field is described by effective charges e_L^* which relate the normal component of the dynamic dipole moment μ_z to the rigid displacements w_L of layer L normal to the surface through,

$$\mu_z = \sum_L e_L^* w_L. \tag{16}$$

Here we use the same model for e_L^* as in Ref. [5],

$$e_1^* = -e_2^* = e^* \quad \text{and} \quad e_L^* = 0, \quad L > 2. \tag{17}$$

Note that a rigid displacement of the metal atoms normal to the surface cannot give rise to a dipole moment, i.e., $\Sigma_L e_L^* = 0$. The projection of the phonon density of states relevant for dipole losses is accordingly given by

$$g(\omega) = \int_0^1 d\zeta \left| \sum_L n_L^* w_L(\zeta) \right|^2 \delta[\omega - \omega(\zeta)] \tag{18}$$

where $n_L^* = e_L^*/e_{tot}^*$, with $e_{tot}^* = (\Sigma_L e_L^{*2})^{1/2}$, is the normalized field of effective charges. The spectral function $S(\omega)$ for the dipole–dipole correlation function appearing in the energy loss function is related to $g(\omega)$ through [18],

$$S(\omega) = [1 + n(\omega)]\, e_{tot}^{*2} \frac{\hbar}{2M\omega}\, g(\omega), \tag{19}$$

where the mass M of a metal atom appears in the root-mean-square amplitude $\hbar/2M\omega$ for phonons with energy $\hbar\omega$ and $n(\omega)$ is the Bose–Einstein distribution factor.

From the inelastic dipole scattering theory the inelastic current $I_1(\omega)$ of electrons collected in the detector around the specular direction after experiencing an energy loss $\hbar\omega$ is given with sufficient accuracy by [17]

$$I_1(\omega)/I_{tot} = \frac{\pi m e^2}{\hbar^2 A E_0 \cos\alpha} f(E_0, \omega, \alpha) S(\omega), \tag{20}$$

where I_{tot} is the total integrated intensity of the elastic peak in the energy loss spectrum, m the electron mass, A the area of the surface primitive cell, and E_0 the kinetic energy of the electron incident with an angle α from the surface normal. The function $f(E_0, \omega, \alpha)$ is given by [17]

$$f(E_0, \omega, \alpha) = (\sin^2\alpha - 2\cos^2\alpha) Y + (\sin^2\alpha + 2\cos^2\alpha) \ln X, \tag{21}$$

where $Y = \theta_1^2/(\theta_1^2 + \theta_0^2)$, $X = (\theta_0^2 + \theta_1^2)/\theta_0^2$, $\theta_0 = \hbar\omega/2E_0$ gives the angular extension of the dipole lobe, and θ_1 the half-angle of the detector aperture. The loss function depicted in Fig. 5 is now obtained from eq. (20) by calculating the projected phonon density of states defined in eq. (18) by the transfer matrix method for the distribution of effective charges given in eq. (17). The parameters α, θ_1, and E_0 are determined from the experimental conditions described in Section 2, and the experimental resolution was introduced by a 4 meV Gaussian broadening of $g(\omega)$. The total effective charge e_{tot}^* had to be chosen to be $0.034e$ and $0.039e$ for Cu and Ni, respectively, in order to reproduce the measured loss intensities at 300 K. These values are of the same order of magnitude as for the value determined previously for the Cu(100) surface [5]. Because the resonance gives rise to a rather sharp loss peak there has been no particular need to have a detailed analysis of the contribution from the

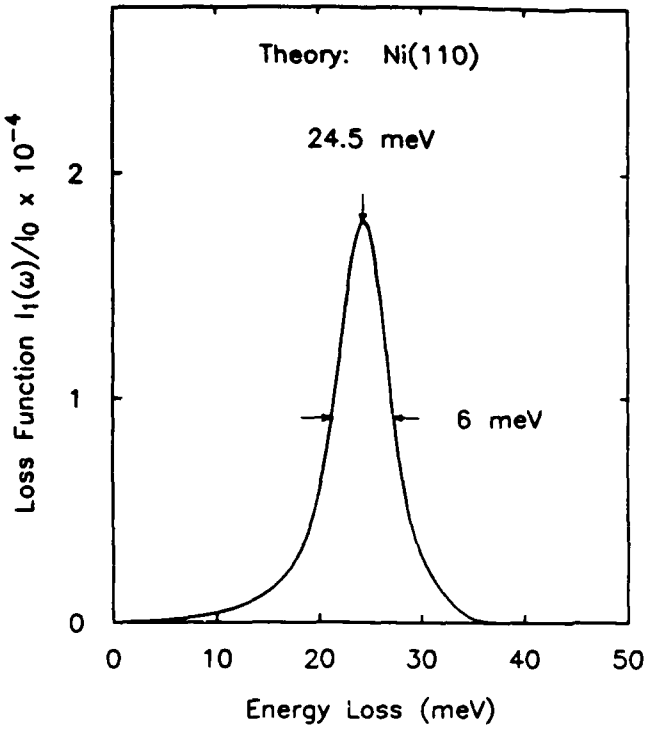

Fig. 5. Calculated electron energy loss function $I_1(\omega)/I_0$ for Ni(110) at 300 K. I_0 is the maximum intensity of the elastic peak in the energy loss spectrum. Only the two outermost surface layers are assumed to be dipole active and the total effective charge e^*_{tot} has been adjusted to $0.039e$ (e is the free electron charge) in order to reproduce the measured loss in Fig. 1. The instrumental resolution has been introduced by a Gaussian broadening of 4 meV.

electron–hole pair excitations to subtract the background [19].

The calculated position of 24.5 meV and the peak width of 6 meV for the surface vibrational resonance are in good agreement with the measured values for Ni. Note that the value for this peak position is about 1 meV higher than for the peak position deduced from $g(\omega)$ for the projection on the outermost layer. This difference is due to the fact that the low energy bulk phonons contribute much less to this dipole active projection, which suppresses the asymmetry of the peak. The peak position is thus closer to the value for the real part of the pole in the complex ω-plane as given in the previous section. For Cu, $g(\omega)$ is obtained in the advocated force constant model simply by scaling the phonon energies with $\omega_0(\mathrm{Cu})/\omega_0(\mathrm{Ni}) \approx 0.81$. This gives an energy of 19.8 meV, in good agreement with the measured value of 20 meV observed in Fig. 1.

There are no reasons to expect that the only effect of the surface is the loss of coordination of atoms in the surface region as described by eq. (17). For instance, both model calculations for the total energy [20] and LEED measurements [8] have shown that the atoms relax oscillatorily in the surface region for many metals. In these new equilibrium positions for the atoms the force constants can be different from the bulk values. Off-specular measurements of the Rayleigh surface phonon dispersion on Ni(100) by EELS have suggested that the interlayer force constant between the first and second layer is about 20% larger than the bulk value [1, 2]. On Ag(111) the observation by inelastic He scattering of a surface vibrational resonance away from the $\bar{\Gamma}$-point in the SBZ could be accounted for by a reduction of about 50% of the radial part of the force constant between atoms in the surface region [3, 4].

The position of the surface vibrational resonance in the observed energy loss spectrum should also contain information about the surface force constants. The sensitivity of the position of the resonance to changes in the surface interlayer force constants has been investigated by calculating a dipole active projection of the phonon density of states $g(\omega)$ for different values of the surface interlayer force constants for Ni. The resonance is predominantly localized in the two outermost surface layers and should accordingly be most sensitive to changes of the interlayer force constants within these layers. The corresponding modification of the interlayer force constants is described by the following equation of motion for the surface layers,

$$\begin{aligned} M\omega^2 w_1 &= \alpha_1(w_1 - w_2) + \alpha_2(w_1 - w_3) \\ M\omega^2 w_2 &= \alpha_1(w_2 - w_1) + \alpha(2w_2 - w_3 - w_4) \\ M\omega^2 w_3 &= \alpha_2(w_3 - w_1) + \alpha(3w_3 - w_2 - w_4 - w_5) \end{aligned} \qquad (22)$$

The resulting position and width of the resonance are tabulated in Table I for a considerable range of values for $R_1 = \alpha_1/\alpha$ and $R_2 = \alpha_2/\alpha$. No attempt has been made to relate these parameters to the observed oscillatory relaxations of this surface since that would require a detailed microscopic model for the interaction potential. It would be possible to proceed with the simple pair potential, but the results obtained would be highly doubtful for a transition metal due to the different characters of the contributions to the interaction energy from the free electron like s-electrons and the tightly bound d-electrons. That the position of the resonance is much more dependent on R_1 than R_2 is no surprise since the displacement field of the resonance has its dominant weight on the relative displacement of the two outermost surface

Table I. *The influence of the surface interlayer force constants on the resonance position and width. The surface interlayer force constants $R_1 = \alpha_1/\alpha$ and $R_2 = \alpha_2/\alpha$ are normalized to the bulk interlayer force constant α. The resonance position ω_{res} and the width Γ_{res} are normalized to the position ω^0_{res} ($= 24.5$ meV for Ni) and width Γ^0_{res} ($= 3.1$ meV for Ni, estimated full width at half maximum) corresponding to the situation $\alpha_1 = \alpha_2 = \alpha$. The area enclosed by the solid line is the range of values in accordance with the observed resonance position when the error bars are taken into account. The dashed entries for the resonance widths indicate that the resonance is no longer well defined*

R_1 R_2	0.6	0.8	1.0	1.2	1.4	1.6
			ω_{res} ω^0_{res}			
0.6	0.79	0.82	0.84	0.87	0.88	0.90
0.8	0.92	0.92	0.93	0.94	0.95	0.97
1.0	1.03	1.00	1.00	1.00	1.01	1.02
1.2	1.08	1.05	1.06	1.06	1.06	1.06
1.4	1.08	1.08	1.08	1.08	1.08	1.08
			Γ_{res} Γ^0_{res}			
0.6	2.5	1.8	1.3	0.9	0.7	0.5
0.8	2.3	1.7	1.2	0.9	0.7	0.5
1.0	1.4	1.2	1.00	0.7	0.6	0.4
1.2		0.5	0.5	0.4	0.4	0.2
1.4						

layers. The experimental resolution is such that it can determine the peak position within 1 meV. The corresponding range for the position of the observed resonance relative to the calculated position is then 0.94 to 1.02 and is enclosed by a solid line in Table I. A large range of values for R_2 is acceptable but not for R_1. The Table suggests that R_1 lies between 0.8 and 1.1. There are also notable changes in the width of the resonance when R_1 and R_2 are changed. For large values of R_1 the resonance emerges into the region of large bulk phonon density of states and the width is no longer well defined. With the present resolution of electron energy loss spectrometers it is not meaningful to extract any information about these parameters from the observed resonance width.

Another consideration to be taken into account is how the effective charges are distributed among the surface layers. In the case of the Cu(100) surface the results from a jellium model calculation for Cu suggested the distribution defined in eq. (17) [5]. The application of the same model for the Cu(110) surface gives, however, that even the third and fourth layers have an appreciable effective charge e_L^* mainly due to a smaller interlayer distance in this direction. In Fig. 6 (lower panel) we present results for $g(\omega)$ calculated for Ni with two different distributions for $n_L^* = e_L^*/e_{tot}^*$ extending to the third and fourth layers and compare with the result from the distribution defined in eq. (17). For the other two distributions the resonance peak is still prominent and does not change its position, but the strength of the states in the upper bulk band region has been appreciably enhanced. The measured loss spectra for Cu and Ni do not indicate such a strong contribution from the bulk states.

Thus our analysis of the loss spectra suggests that there are no dramatic changes in the surface interlayer force constants from the bulk values.

5. Dispersion of the resonance along the $\bar{\Gamma}$–$\bar{X}$ direction

The dispersion of surface vibrational modes along different directions in the SBZ has been shown to be feasible to measure for a few metal surfaces by inelastic He scattering [3] and off-specular EELS [1]. Therefore it is of interest to know how the resonance disperses away from the $\bar{\Gamma}$-point. It is found that the resonance exists and is derived from a pseudo-band gap even out to the $\bar{X}$-point. The resonance makes an avoided crossing with another resonance derived from a surface phonon in a bulk band gap. Close to the $\bar{X}$-point the resonance leaves the bulk subbands and appears as a surface phonon.

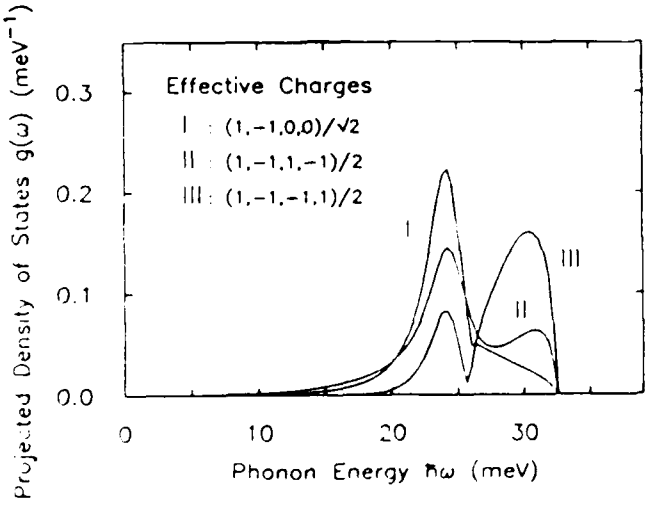

Fig. 6. Sensitivity of $g(\omega)$ to different models for the effective charge fields. Results for different choices of the effective charges (e_1^*, e_2^*, e_3^*, e_4^*) of the four outermost surface layers are shown. $e_{tot}^* = 1$ when $z_1 = z_2 = z$.

Along the $\bar{\Gamma}$–$\bar{X}$ direction the displacements of the atoms partition into two classes due to the reflection plane symmetry. The odd modes are polarized in the y-direction and are symmetry forbidden to couple with displacements of atoms polarized in the x–z plane which form the even class. In the nearest neighboring central force constant model the motion of atoms in the y-direction gives rise to a monotonic dispersion of the corresponding phonons with no pseudoband gaps. Henceforth the y-motion will not be considered further. The equations of motion for displacements of atoms in the x-direction and in the z-direction are coupled along the $\bar{\Gamma}$–$\bar{X}$ direction and are for the bulk layers given by

$$\begin{aligned}\omega^2 u_L &= \frac{\alpha}{M}[(4 - 2\cos(\pi\xi))u_L - \cos(\pi\xi/2)(u_{L-1} + u_{L+1}) \\ &\quad + i\sin(\pi\xi/2)(w_{L+1} - w_{L-1})], \\ \omega^2 w_L &= \frac{\alpha}{M}[4w_L - \cos(\pi\xi/2)(w_{L+1} + w_{L-1}) \\ &\quad - (w_{L+2} + w_{L-2}) + i\sin(\pi\xi/2)(u_{L+1} - u_{L-1})],\end{aligned} \tag{23}$$

where $u_L\, e^{i(k_x R_x - \omega t)}$ and $w_L\, e^{i(k_x R_x - \omega t)}$ are displacements in the x- and z-directions, respectively, of an atom at position $\boldsymbol{R}$ in Layer L, and $\xi = k_x a/\sqrt{2\pi}$ is the reduced wavevector along the $\bar{\Gamma}$–$\bar{X}$ direction. At the point $\bar{\Gamma}$-point ($\xi = 0$) the equations of motion for u_L and w_L are decoupled and eq. (1) is recovered for w_L.

The solutions to eq. (23) are plane waves $u_L = u(\xi, \zeta)\, e^{i\pi\zeta L}$ and $w_L = w(\xi, \zeta)\, e^{i\pi\zeta L}$ which would result in two branches of the dispersion relation, one lower $\omega_l = \omega_l(\xi, \zeta)$ and one upper $\omega_u = \omega_u(\xi, \zeta)$. The behavior of these two branches at $\xi = 0.6$ is illustrated in Fig. 7. If one artificially removes the coupling between u_L and w_L then the dispersion for phonons polarized in the x-direction is monotonic and crosses twice the dispersion for phonons polarized in the z-direction. The latter dispersion is non-monotonic due to the strong coupling to the second nearest neighboring layer. The coupling present in eq. (23) between u_L and w_L causes these two branches to make two avoided crossings with corresponding interchange of character and makes them both non-monotonic with ζ.

The influence of the surface on the force constants is modeled in the same way as in Section 3 by taking into account only the loss of coordination of atoms in the surface region. In this complex case we will not attempt to write out the form of the scattered wave for an incident wave. It is much more tractable to generate results for the surface vibrational density of states by using the transfer matrix method. This method cannot be applied directly to this system, however, due to the fact that the dynamical submatrix D between the principal layers is singular (see Appendix). This matrix D_{01} can be regularized, however, by introducing a small second layer coupling $(\alpha/M)r(u_{L-2} + u_{L-2})$ into the equations of motion for u_L in eq. (23). The values of $r = 0.01$ is found to be sufficiently small for an accurate calculation of the phonon density of states. This value for r is much smaller than the errors in the nearest neighboring force constant model used to describe Cu and Ni.

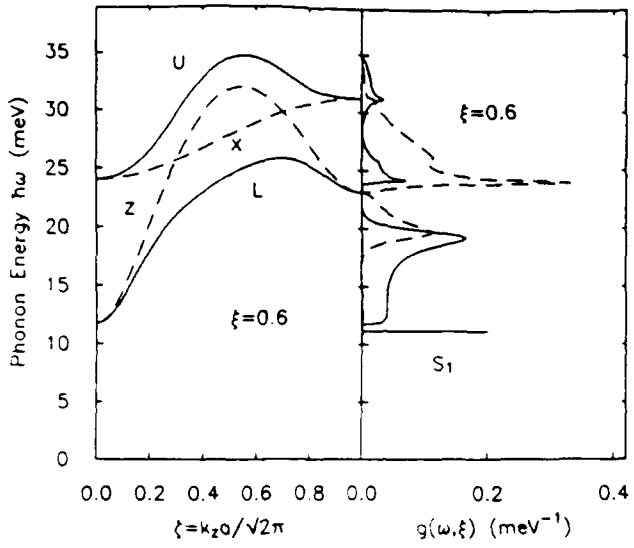

Fig. 7. Dispersion of bulk phonons in the [110] direction of Ni and the corresponding surface phonon density of states $g(\omega)$ at $\xi = k_z a/\sqrt{2}\pi = 0.6$. The left panel shows the two branches, an upper "U" and a lower "L" branch, of the dispersion in the [110] direction (solid lines) arising from an avoided crossing between phonons polarized in the x- and z-directions, respectively. The dashed lines show the dispersion when the interaction between these two polarizations is turned off. The right panel shows the phonon density of states $g(\omega)$ projected on the z-motion (solid line) and the x-motion (dashed line) of the outermost surface layer.

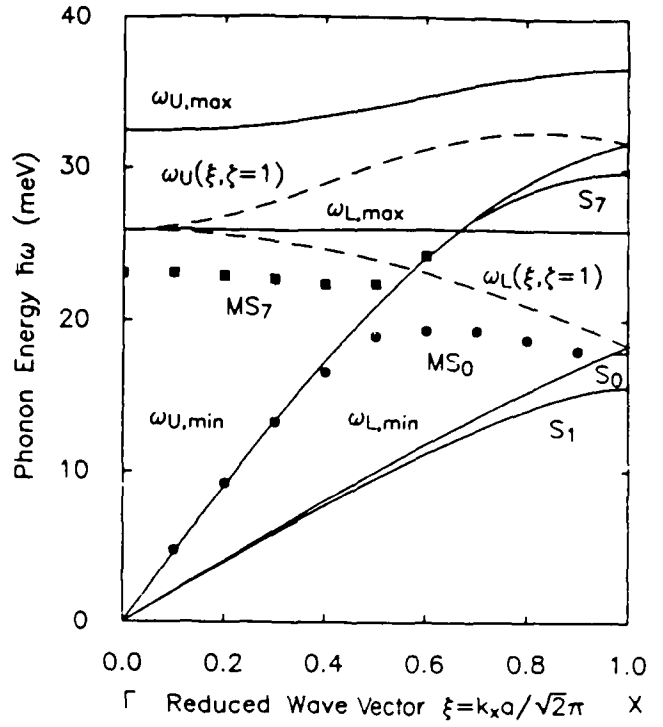

Fig. 8. Dispersion of the resonance along the $\Gamma\bar{X}$-direction. The dispersion of the resonance arising from the pseudoband gap (squares) makes an avoided crossing with the dispersion of the resonance (circles) derived from the $S_7(\bar{X})$ surface phonon. The solid lines give the maximum $\hbar\omega_{t,max}$, $\hbar\omega_{l,max}$ and minimum $\hbar\omega_{t,min}$, $\hbar\omega_{l,min}$ energies of the lower and the upper boundaries of bulk subbands, respectively. The dashed lines show $\hbar\omega_t(\xi, \zeta = 1)$ and $\hbar\omega_l(\xi, \zeta = 1)$ for phonons with a dashed wavevector $\xi = k_x a/\sqrt{2}\pi$ where a is the lattice constant. The notation of the surface phonons S_i and S_7 are taken from Ref. [21].

The results in Fig. 7 for the phonon density of states $g(\omega, \xi)$ at $\xi = 0.6$ projected on the x-motion and the z-motion of the outermost layer show several prominent features. There is a localized state in the gap at 11.1 meV, the surface phonon S_1 in the notation of Ref. [21], being split off from the bulk subbands by the reduction of the restoring forces in the surface region. The x-projection of $g(\omega, \xi)$ shows a narrow peak at 24 meV just below the minimum energy of the upper branch which can be interpreted as a state being split off from the upper branch and turning into a resonance due to overlap with states in the lower branch. Thus the origin of this resonance is the same as for the resonance discussed in the work on Ag(111) where an "anomalous" peak was observed in inelastic He scattering [3]. There is, however, another narrow peak in the z-projection of $g(\omega, \xi)$ around 19 meV. The non-monotonic behavior of the lower branch suggests the interpretation that this peak is a resonance derived from the corresponding pseudoband gap of the lower branch below $\omega_t(\xi, \zeta = 1)$. The upper branch shows similar non-monotonic behavior with a pseudoband gap in between $\omega_{u,min}$ and $\omega_u(\xi, \zeta = 1)$ which results in a resonance at 31.1 meV, very close to $\omega_u(\xi, \zeta = 1)$. However, its dominant amplitudes are on layers further inside the surface.

By calculating the x- and z-projections of $g(\omega, \xi)$ on the outermost layer for several values of ξ between 0 and 1 the behavior of the surface vibrational modes can be followed along the $\Gamma\bar{X}$ direction as shown in Fig. 8. At the $\bar{X}$-point we have three surface phonons for displacements polarized in the x–z plane (i) S_1 the Rayleigh surface phonon (ii) S_u which exists only close to $\bar{X}$ and (iii) S_7 a gap mode. The labelling of the modes are taken from Ref. [21] except for S_u which was not identified in their slab calculations. The mode S_7 is localized on the second and third layer and is predominantly polarized in the z-direction. This mode turns into a resonance MS_7 inside the lower bulk subband and lies in the pseudoband gap just below $\omega_t(\xi, \zeta = 1)$. At around $\xi = 0.5$–0.6 the resonance interacts with the MS_7 resonance and makes an avoided crossing with a corresponding interchange of character. The resonance MS_7 is a continuation of the gap mode S_7 into the bulk subbands and becomes mainly polarized in the x-direction for $0.6 < \xi \leq 1.0$. When ξ approaches the $\bar{\Gamma}$-point ($\xi = 0$) MS_7 goes over into the resonance discussed in the previous sections and is mainly polarized in the z-direction. From the $\bar{\Gamma}$-point to the avoided crossing the width of MS_7 remains roughly the same (about 3.5 meV) and after it interchanges character it sharpens appreciable to a width less than 0.5 meV. MS_0 broadens and gets more localized on the outermost layer away from the $\bar{\Gamma}$-point and just at the crossing the width is about 2 meV. After the crossing the width remains about the same and sharpens up only just before leaving the bulk subband. Thus at the crossing the widths of the resonances overlap, which makes the avoided crossing less well defined.

6. Summary

A new kind of surface vibrational resonance is shown from surface lattice dynamics to exist on surfaces having a pseudoband gap in the bulk phonon density of states. The surface splits off a mode from a region of high density of states into a pseudoband gap region where the density of states is largely depleted. This behavior is illustrated for phonons having a surface component of the wavevector along the $\bar{\Gamma}\bar{X}$ direction in the SBZ of the (110) surfaces of Cu and Ni. Recent measurements and analysis of the Fe bcc (111) surface have shown this type of resonance to be a general effect [7]. In these

cases, the pseudoband gap is a geometric structure effect caused by the particular coordination of the atoms, which leads to higher Fourier components in the non-monotonic bulk phonon dispersion relations.

At the $\bar{\Gamma}$-point the resonance is dipole active and has been observed by EELS on the (110) surface of Cu and Ni and the (111) surface of Fe [7]. From these observations it has been possible to obtain some information on the surface interlayer force constants. In particular, the positions of the loss peak can only be reproduced for Ni when the outermost surface interlayer force constant lies within -20% to 10% of the bulk value. Along the $\bar{\Gamma}\bar{X}$ direction in the SBZ of Cu and Ni the resonance makes an avoided crossing with a resonance derived from the $S_3(\bar{X})$ surface phonon. This novel behavior should be possible to observe by inelastic electron or He scattering at large parallel wavevector transfers.

Finally, this analysis suggests in general that this type of surface vibrational resonance should be observable not only by inelastic electron dipole scattering but by other surface spectroscopies, such as inelastic He scattering, on a variety of surfaces at points in the SBZ where a bulk phonon dispersion is non-monotonic and consequently has a pseudoband gap. The origin of these effects is directly related to the geometric structure of the surface.

Acknowledgements

Support of this research by the Office of Naval Research, under Contracts No. N00014-81-K-0505 and N00014-82-K-0576, and the Swedish Natural Science Research Council is gratefully acknowledged. It is a pleasure to thank Mark Stiles and John Wilkins for stimulating discussions during the course of this work.

Appendix

In this Appendix it is shown how the transfer matrix method proposed by Lee and Joannopoulos [12] can be applied to the calculation of surface vibrational density of states. The method is illustrated for the surface lattice dynamics problem of longitudinal phonons propagating normal to a fcc (110) surface. Furthermore, this method justifies the choice of the ansatz for the scattered waves in eqs. (9) and (14).

The first step in this method is to form principal layers, here labelled by an integer n, $n = 1, 2, \ldots$, from the layers of atoms parallel to the surface such that the dynamical matrix only introduces interactions between displacement fields in nearest neighboring principal layers. In the present case two layers form a principal layer. The column vector W_n denotes displacement fields in the principal layer n,

$$W_n(i) = w_{2n+i-2}, \quad i = 1, 2. \tag{A1}$$

In terms of these column vectors W_n the eigenvalue problem for the bulk layers can be written as,

$$(z - D_{00})W_n - D_{01}W_{n+1} - D_{01}^{\dagger}W_{n-1} = 0, \quad n = 1, 2, \ldots, \tag{A2}$$

and the corresponding equation for the surface layers is given by,

$$(z - D_{s0})W_1 - D_{01}W_2 = 0. \tag{A3}$$

Here $z = \omega^2$ and D_{00}, D_{01} and D_{s0} are (2×2) dynamical submatrices formed from the full dynamical matrix $D(L, L')$ which can be obtained directly from eqs. (1) and (7). $D_{00}(i, j) = D(2L + i - 2, 2L + j - 2)$, $D_{01}(i, j) = D(2L + i - 2, 2L + j)$. L denotes a bulk layer, and $D_{s0}(i, j) = D(i, j)$. For instance, D_{01} is given by,

$$D_{01} = \frac{\chi}{M}\begin{pmatrix} 1 & 0 \\ 1 & 1 \end{pmatrix}. \tag{A4}$$

Equation (A2) shows explicitly that there are only interactions between displacement fields in nearest neighboring principal layers. Since D_{01}^{-1} exists W_{n+1} can be directly expressed in terms of the two preceding column vectors W_n and W_{n-1} by a simple rearrangement of eq. (A2) as,

$$W_{n+1} = D_{01}^{-1}(z - D_{00})W_n - D_{01}^{-1}D_{01}^{\dagger}W_{n-1}, \quad n = 2, 3, \ldots. \tag{A5}$$

This equation shows that it is possible to construct a matrix $T(z)$ which relates the displacement fields in two principal layers $n + 2$ and $n + 1$ to the corresponding fields in the two preceding principal layers n and $n - 1$,

$$\begin{pmatrix} W_{n+2} \\ W_{n+1} \end{pmatrix} = T(z)\begin{pmatrix} W_n \\ W_{n-1} \end{pmatrix}. \tag{A6}$$

The matrix $T(z)$ is the transfer matrix and is given by the product of the following two matrices,

$$T(z) = \begin{pmatrix} D_{01}^{-1}(z - D_{00}) & -D_{01}^{-1}D_{01}^{\dagger} \\ 1 & 0 \end{pmatrix} \times \begin{pmatrix} D_{01}^{-1}(z - D_{00}) & -D_{01}^{-1}D_{01}^{\dagger} \\ 1 & 0 \end{pmatrix} \tag{A7}$$

By iterating eq. (A6), a displacement field in any principal layer can be determined from their values on the surface layers as,

$$\begin{pmatrix} W_{n+2} \\ W_{n+1} \end{pmatrix} = T^n(z)\begin{pmatrix} W_2 \\ W_1 \end{pmatrix}. \tag{A8}$$

Equation (A3) for W_2 and W_1 gives only 2 equations for 4 displacement fields and are not sufficient to determine W_2 and W_1. Further restrictions are found by introducing the appropriate boundary conditions. That can be done by analyzing the eigenvalues and eigenvectors of the dynamical matrix.

For the bulk layers the solution of eq. (A2) is given by translational symmetry as plane waves,

$$W_n = \begin{pmatrix} e^{i2\pi n\zeta} \\ e^{i2\pi(n-1)\pi\zeta} \end{pmatrix}, \tag{A9}$$

where the reduced wavevector ζ satisfies the bulk dispersion relation $\omega^2 = \omega_0^2[\sin^2(\pi\zeta/2) + \sin^2(\pi\zeta)]$ as given by eq. (3) in Section 3. In terms of the variable $\lambda = e^{i\pi\zeta}$ this dispersion relation is equivalent to a polynomial of degree 4 in λ and has accordingly 4 roots λ_k, $k = 1, 2, 3, 4$. The eigenvectors $V_k(z)$ of $T(z)$ can now be directly formed from this plane wave solutions,

$$V_k(z) = \begin{pmatrix} \lambda_k^3 \\ \lambda_k^2 \\ \lambda_k \\ 1 \end{pmatrix} \tag{A10}$$

and the associated eigenvalue for $V_k(z)$ is given by λ_k^4 and

$T(z)V_k = \lambda_k^4 V_k$. The eigenvalues are distinct away from the critical points, $d\omega/d\zeta = 0$, and the corresponding eigenvectors span the 4-dimensional space of displacement fields of two adjacent principal layers. Thus W_2 and W_1 can then be simultaneously expanded in terms of V_k,

$$\begin{pmatrix} W_2 \\ W_1 \end{pmatrix} = \sum_{k=1}^{4} c_k V_k. \tag{A11}$$

This equation and eq. (A8) give directly that the displacement field for any principal layer can be expressed as,

$$\begin{pmatrix} W_{2n+2} \\ W_{2n+1} \end{pmatrix} = \sum_{k=1}^{4} c_k \lambda_k^{4n} V_k, \quad n = 0, 1, 2, \ldots, \tag{A12}$$

or in terms of the displacement field w_L for a layer L,

$$w_L = \sum_{k=1}^{4} \tilde{c}_k \, e^{i\pi\zeta_k L}, \tag{A13}$$

where $\tilde{c}_k = c_k \, e^{-i2\pi\zeta_k}$. This form of solution in eq. (A13) justifies the ansatz made in eqs. (9) and (14) in Section 3. The solution corresponding to scattered wave can be found by imposing the outgoing boundary conditions as discussed in Section 3. This restricts the solutions to depend on two parameters. These two parameters can then be determined from the two equations for the surface layers.

A more convenient way to evaluate the vibrational density of states $g(\omega, \{n_L\})$ than using the scattered wave solutions appearing in eq. (A13) is to determine first the resolvent matrix (a Green's function) $U(L, L'; z)$ associated with the dynamical matrix $D(L, L')$. This resolvent is defined by,

$$\sum_{L''} [z\delta(L, L'') - D(L, L'')]U(L'', L'; z) = \delta(L, L'), \tag{A14}$$

and the vibrational density of states is given by,

$$g(\omega, \{n_L\}) = -\frac{2\omega}{\pi} \operatorname{Im} \sum_{L,L'} n_L U(L, L'; (\omega + i0^+)^2) n_{L'}. \tag{A15}$$

The transfer matrix approach can now be applied by considering the resolvent (2×2) submatrices $U_{n,n}(z)$ with respect to the principal layers and they are defined as,

$$U_{n,n}(i, j; z) = U(2n - L + i, 2n' + L - j; z), \quad i, j = 1, 2. \tag{A16}$$

To obtain the vibrational density of states for the surface layers it is sufficient to evaluate $U_{1,1}(z)$. The resolvent matrix element $U_{n,1}(z)$ satisfies the same equations as W_n, eq. (A2), except at the surface layers where the equations have an inhomogeneous term,

$$(z - D_{00})U_{1,1}(z) - D_{01}U_{2,1}(z) = 1 \tag{A17}$$

Similar to the construction of W_n, $U_{n,1}(z)$ can be constructed from $U_{1,1}(z)$ and $U_{2,1}(z)$ by iterating the transfer matrix,

$$\begin{pmatrix} U_{2n+2,1}(z) \\ U_{2n+1,1}(z) \end{pmatrix} = T^n(z) \begin{pmatrix} U_{2,1}(z) \\ U_{1,1}(z) \end{pmatrix}. \tag{A18}$$

Some care is needed to get the correct physical Riemann sheet of the resolvent as a function of z. On this sheet $U_{n,1}(z)$ has to be decaying with n when imparting a small positive imaginary part $i\varepsilon$ to ω, $z = (\omega + i\varepsilon)^2$. Such a decay is evidently achieved by expanding the two column vectors of $U_{2,1}(z)$ and $U_{1,1}(z)$ simultaneously in terms of those eigenvectors with $|\lambda_k| < 1$. This point and the fact that for complex z the eigenvectors are divided evenly into two classes $|\lambda_k| < 1$ and $|\lambda_k| > 1$, respectively, were shown in detail for the general case in the original work by Lee and Joannopoulos [12]. Let $k = 1, 2$ label the two eigenvectors with $|\lambda_k| < 1$ and introduce the two associated (2×2) matrices,

$$\begin{aligned} W_U(i, j) &= V_j(i) \\ W_L(i, j) &= V_j(i + 2). \end{aligned} \tag{A19}$$

The expansion of the two submatrices of the resolvent in these two eigenvectors now becomes,

$$\begin{pmatrix} U_{2,1}(z) \\ U_{1,1}(z) \end{pmatrix} = \begin{pmatrix} W_U A \\ W_L A \end{pmatrix} \tag{A20}$$

where the coefficients in the expansion forms a (2×2) matrix A. These two resolvents are now specified by 4 parameters. The 4 surface layer equations in eq. (A17) for $U_{1,1}(z)$ and $U_{2,1}(z)$ will now completely determine these parameters. This can be done by first eliminating the matrix A from eq. (A20).

$$U_{2,1}(z) = W_U W_L^{-1} U_{1,1}(z). \tag{A21}$$

Furthermore, by inserting this expression for $U_{2,1}(z)$ into eq. (A17) a simple linear matrix equation is obtained for $U_{1,1}(z)$ which can be solved by a matrix inversion,

$$U_{1,1}(z) = (z - D_{00} - D_{01} W_U W_L^{-1})^{-1}. \tag{A22}$$

Thus for every frequency ω the vibrational density of states can be evaluated from eqs. (A15) and (A22) by diagonalization of a (4×4) complex matrix and by inversion of two (2×2) matrices. $U_{1,1}(z)$ will have simple poles at those frequencies corresponding to localized vibrational modes at the surface. Similarly, the resonances appear as poles in the complex frequency plane but not on the physical Riemann sheet of $U_{1,1}(z)$. However, the other Riemann sheets of $U_{1,1}(z)$ should be possible to construct from other choices for the eigenvectors in eq. (A19).

References

1. Lehwald, S., Szeftel, J. M., Biach, H., Rahman, T. S. and Mills, D. L., Phys. Rev. Lett. **50**, 518 (1983); Rocca, M., Lehwald, S., Ibach, H. and Rahman, T. S., Surf. Sci. **138**, 1123 (1984).
2. Xu, M.-L., Hall, B. M., Tong, S. Y., Rocca, M., Ibach, H., Lehwald, S. and Black, J. E., Phys. Rev. Lett. **54**, 1171 (1985).
3. Doak, R. B., Harten, U. and Toennies, J. P., Phys. Rev. Lett. **51**, 578 (1983).
4. Bortolani, V., Franchini, A., Nizzoli, F. and Santoro, G., Phys. Rev. Lett. **52**, 429 (1984).
5. Andersson, S., Persson, B. N. J., Persson, M. and Lang, N. D., Phys. Rev. Lett. **52**, 2073 (1984).
6. Stroscio, J. A., Persson, M., Bare, S. R. and Ho, W., Phys. Rev. Lett. **54**, 1428 (1984).
7. Stroscio, J. A., Persson, M., Bartosch, C. E. and Ho, W., Phys. Rev. **B33**, 2879 (1986).
8. For a recent compilation of data see: Gauthier, Y., Baudoing, R., Joly, Y., Gaubert, C. and Rundgren, J., J. Phys. **C17**, 4547 (1984).
9. Bortolani, V., Franchini, A., Garcia, N., Nizzoli, F. and Santoro, G., Phys. Rev. **B28**, 7358 (1983).
10. Svensson, E. C., Brockhouse, B. N. and Rowe, J. M., Phys. Rev. **155**, 619 (1967).
11. Birgenau, R. J., Cordes, J., Dolling, G. and Woods, A. D. B., Phys. Rev. **136**, A1359 (1964).

12. Lee, D. H. and Joannopoulos, J. D., Phys. Rev. **B23**, 4997 (1981).
13. Stroscio, J. A., Bare, S. R. and Ho, W., Surf. Sci. **148**, 499 (1984).
14. Ho, W., Willis, R. F. and Plummer, E. W., Phys. Rev. Lett. **40**, 1463 (1978); Phys. Rev. **B21**, 4202 (1980).
15. Maradudin, A. A., Montroll, E. W., Weiss, G. H. and Ipatore, I. P., Lattice Dynamics in the Harmonic Approximation, 2nd edition, Academic, New York (1981).
16. Fano, U., Phys. Rev. **124**, 1866 (1961).
17. Ibach, H. and Mills, D. L., Electron-Energy-Loss Spectroscopy and Surface Vibrations. Academic, New York (1982).
18. Persson, M., Physica Scripta **29**, 181 (1984).
19. Andersson, S. and Persson, B. N. J., Phys. Rev. Lett. **50**, 2028 (1983).
20. Finnis, M. W. and Heine, V., J. Phys. **F4**, L37 (1974); Landmann, U., Hill, R. N. and Mostoller, M., Phys. Rev. **B21**, 448 (1980); Barnett, R. N., Landmann, U. and Cleveland, C. L., Phys. Rev. Lett. **51**, 1359 (1983).
21. Allen, R. E., Alldredge, G. P. and deWette, F. W., Phys. Rev. **B4**, 1661 (1971).

END

FEB.

1988

DTIC